Effect of Salinity on Water/Oil Interface with Model Asphaltene and Non-Ionic Surfactants: Insights from Molecular Simulations

Xiaoyu Sun[†], Hongbo Zeng[,†], Tian Tang[*,‡]*

[†]Department of Chemical and Materials Engineering, University of Alberta, Edmonton, AB T6G 1H9, Canada

[‡]Department of Mechanical Engineering, University of Alberta, Edmonton, AB T6G 1H9, Canada

** Corresponding authors:*

E-mail: hongbo.zeng@ualberta.ca (H.Z.); Phone: +1-780-492-1044;

E-mail: tian.tang@ualberta.ca (T.T.); Phone: +1-780-492-5467.

Abstract

Water or brine always co-exist with oil during petroleum production, often in the form of emulsions which can be stabilized by surface-active components such as asphaltenes. Polymeric demulsifiers were frequently applied to destabilize the water/oil interface. To understand the demulsification mechanisms of water/oil emulsion, it is important to understand the effect of salinity on the stability of water/oil interface with adsorbed asphaltenes and polymeric demulsifiers. In this work, molecular dynamics simulations were performed on water/heptol interfaces under the influence of a model asphaltene (VO-79), a polymer demulsifier (PEO_5-PPO_{10}-PEO_5) and varying concentrations of NaCl. Potential of mean force calculation indicated that when NaCl was added the magnitude of the adsorption free energy for VO-79 had insignificant changes and that for the polymer increased. In the absence of VO-79, the interfacial tension (IFT) at the water/heptol interface first increased upon increasing the NaCl concentration to 6 wt.% and then decreased. The initial increase was attributed to the negative surface excess of salt while the subsequent decrease was due to the evident aggregation of salt ions in the water phase. With both polymer and VO-79 at the interface, the effect of salinity on IFT followed the same non-monotonic trend, except that the transition occurred at a lower concentration, which was caused by the mutual influence of H-bonds between adsorbates and water, and the surface excess of salt. The results provide useful insights into the effect of salinity on the stabilization and destabilization of water/oil interface.

Keywords: Molecular simulations; Non-ionic surfactant; Water-in-oil emulsions; Demulsification; Effect of salt

1. Introduction

Brine water is always co-produced with oil during petroleum production. [1–3] Low salinity waterflooding is commonly used in enhanced oil recovery (EOR), and different mechanisms have been proposed to contribute to EOR, such as fines migration [4], wettability alteration [5], change of oil-brine interfacial viscoelasticity [6], etc. The produced water from oil production may be recycled, resulting in the accumulation of ions. [7] Thus, the salinity of brine water can range from low in fresh water to high in formation water. [8] The salt in brine water can affect many processes during oil production, including oil recovery and water/oil separation. [1,8,9] In addition, brine water could be stabilized by surface-active components in crude oil, leading to the formation of water-in-oil emulsions. [2] Stable water-in-oil emulsion has attracted wide attention and its treatment is still a big challenge for the petroleum industry. [2] Asphaltenes are the heaviest and most polar components in crude oil, which tend to adsorb at the water/oil interface. [2] The formation of rigid asphaltene films at the water/oil interface was considered the main contributor to the stabilization of water-in-oil emulsions. [10,11] Demulsifiers, such as polymeric surfactants, have been commonly used to destabilize the water/oil interface and promote water/oil separation. Given the ubiquitous presence of salt in the water phase, it is important to understand the interfacial behaviors of asphaltenes and demulsifiers at the water/oil interface under the influence of salinity.

At the interfaces between water and pure hydrocarbon, the interfacial tension (IFT) was reported to increase with salt concentration. [8] Meanwhile, the adsorption of asphaltenes tended to cause the reduction of IFT at the water/oil interface. [12] With asphaltenes at the water/pentol interface, the IFT was found by Xie et al. to increase with NaCl concentration in water from 0 to 3 M. [13] On the other hand, by measuring the IFT at the water/crude oil interface and the size of water-in-oil emulsion droplets, Ling et al. [14] reported that when the NaCl concentration

increased, the IFT decreased and the water droplets were more stable, which were attributed to the interfacial accumulation of surface-active components induced by salt. [14] The viscoelastic properties of the water/crude oil interface were also altered by the addition of NaCl, where high salinity increased the rigidity of the interfacial films. [15] Different types of salt can have different effects on the property of the water/oil interface. Kakati et al. reported that monovalent salts were more effective in reducing IFT for the aliphatic hydrocarbon/brine interface, whereas divalent salts were more effective in reducing IFT for the aromatic hydrocarbon/brine interface. [9] Lashkarbolooki et al. found that the effect of monovalent salt (NaCl) on IFT at asphaltene-in-toluene/water interface was insignificant but the effect of divalent salts ($CaCl_2$ and $MgCl_2$) was evident. [16] At the interface of heavy crude oil and water, $CaCl_2$ was reported to cause higher IFT values than NaCl; in addition, the IFT first decreased and then increased with the concentration of $CaCl_2$. [17] Rostami et al. tested the IFT between crude oil and brine water containing mixed salts (NaCl, $CaCl_2$, $MgCl_2$ etc.). The IFT was found to first decrease and then increase with the salt concentration, which was explained by proposing that the IFT reached the minimum when the interfacial adsorption of asphaltene was saturated. [5] With further increase of salt concentration, the cations accumulated at the interface which interfered with the interaction between water and asphaltenes thus hindering asphaltenes adsorption. [5] Besides IFT, the water/oil interfacial rheology could also be affected by the presence of salt. Chávez-Miyauchi et al. stated that the viscoelasticity of water/crude oil interface might have a non-monotonic (increase-decrease) trend with the concentration of salts (NaCl and $MgCl_2$). [18] Rezaei et al. investigated the stability of emulsions formed by brine in crude oil. Tighter emulsions (more stable with finer droplets) were formed with the brine containing low concentration of KCl, as compared to the brine containing higher concentration of NaCl, KCl, $CaCl_2$, and $MgCl_2$ mixture. [19] Though considerable

experimental efforts have been spent, it remains difficult to find consistent correlations between salinity and interfacial properties of water/oil interface, due to the complexity of oil compositions. [8]

When demulsifiers were added to destabilize water-in-oil emulsion, the effect of salt on the interfacial behaviors became more complex. Zaki et al. studied the demulsification efficiency of PPO-PEO copolymers on water-in-benzene emulsions stabilized by asphaltenes, and observed that the demulsification efficiency decreased with the increase of NaCl concentration from 0 to 1 M. [20] On the contrary, Borges et al. proposed that the increase of NaCl concentration would enhance the adsorption of non-ionic demulsifiers (an ethoxylated iso-tridecanol) at the interface, and thus improve the demulsification efficiency. [21] In Chávez-Miyauchi et al., when a small amount of non-ionic surfactant (an ethoxylated resin) was added, the non-monotonic dependence of interfacial viscoelasticity on salt concentration diminished. [18] The effect of salt concentration therefore appears to vary between different demulsifiers. PPO-PEO copolymers, commonly used as demulsifiers, have been extensively studied, yet their demulsification mechanism, especially under the influence of salt, is not well understood.

Molecular dynamics (MD) simulations have been used to study the interfacial behaviors of asphaltenes at the water/oil interface. The nanoaggregation and thin film formation of asphaltenes, and asphaltene film destruction by ethyl cellulose were observed by MD simulations. [22–25] Alhosani et al. performed MD simulations to study the effect of salt type (NaCl, $CaCl_2$, Na_2SO_4 and Na_2CO_3) and concentration on the interface between water and a toluene/n-dodecane mixture. [26] They observed that the salt ions were depleted at the interface, and that divalent ions (e.g., SO_4^{-2} and CO_3^{-2}) had less tendency to migrate to the bulk oil phase compared with monovalent ions (Na^+ and Cl^-). [26] Jian et al. reported that the IFT of the water/toluene interface increased as

the NaCl concentration increased from 0 to 28 wt.%. [27] With the presence of a model asphaltene (Violanthrone-79, VO-79), the IFT was reduced compared with the pure water/toluene system. [27] The IFT also increased with NaCl concentration, but the increment was less significant compared with the systems without VO-79. [27] Interfacial behaviors of asphaltenes [28], surfactants [29], polymers [30], and sodium naphthenates [31], were also studied by dissipative particle dynamics simulations. To the best of our knowledge, theoretical studies on the effect of salt with the presence of both asphaltene and demulsifier have been absent, but they are essential for the understanding of demulsification mechanisms.

In this work, MD simulations were performed to investigate brine/heptol (mixture of heptane and toluene) interface with the presence of a model asphaltene (VO-79) and a model demulsifier (PEO-PPO-PEO copolymer), while under the influence of a monovalent salt (NaCl). The IFT of a brine/heptol interface was calculated with various concentrations (1.2 wt% - 11 wt.%) of NaCl in the aqueous phase. These simulations mimic the scenario where water-in-oil emulsions are being demulsified, and aim to unravel the effect of salt and demulsifiers on the stability of the brine/heptol interface. The IFT calculations were accompanied by the evaluation of the potential of mean force (PMF) that quantified the adsorption free energy of a single asphaltene or demulsifying polymer. The results provide useful insights into the effect of salinity on the stabilization and destabilization of water/oil interface.

2. Methods

2.1 IFT calculation.

MD simulations were performed on five sets of systems involving water/heptol interfaces (Table 1): control systems without any adsorbates (sys. C_S0 – C_S3), systems with interfacially

adsorbed PEO-PPO-PEO polymers (PEO_5-PPO_{10}-PEO_5, hereafter referred to as "polymers" for simplicity) at low (sys. P97_S0 – P97_S3) or high concentrations (sys. P198_S0 – P198_S3), systems with polymers and pre-adsorbed VO-79 where the polymer concentration was low (sys. VP97_S0 – VP97_S3) or high (sys. VP198_S0 – VP198_S3). Heptol 75/25 (75% vol. heptane, 25% vol. toluene) was used to represent the oil phase as the solubility of asphaltene in this mixture was similar to that in the naphtha-based solvent for froth treatment. [32,33] In sys. C_S0 – C_S3, a cubic box ($7\times7\times7$ nm^3) of heptol 75/25 was built and equilibrated to a final density of 727 kg/m^3, then the box was extended along z-direction to $7\times7\times14$ nm^3, as shown in Supporting Information (SI) section SI1. A cubic box with water molecules was placed into the extended volume, where there was no NaCl in sys. C_S0, 1.2% wt. NaCl in sys. C_S1, 6% wt. NaCl in sys. C_S2, and 11% wt. NaCl in sys. C_S3. The concentration of NaCl was obtained by replacing an appropriate amount of water molecules with Na^+ and Cl^- ions.

Table 1. Details for the simulated systems.

sys.	Summary	Type of simulation
P1_S0 - P1_S3	A single polymer, different NaCl concentrations	SMD, PMF
V1_S0 - V1_S3	A single VO-79, different NaCl concentrations	SMD, PMF
C_S0 - C_S3	No polymer or VO-79, different NaCl concentrations	Non-restrained MD
P97_S0 - P97_S3	97 polymers, no VO-79, different NaCl concentrations	Non-restrained MD
P198_S0 - P198_S3	198 polymers, no VO-79, different NaCl concentrations	Non-restrained MD
VP97_S0 - VP97_S3	97 polymers, 188 VO79, different NaCl concentrations	Non-restrained MD
VP198_S0 - VP198_S3	198 polymers, 188 VO-79, different NaCl concentrations	Non-restrained MD

Note: For system, the number in the name after "S" represents different salt concentrations: S0 - no salt, S1 - 1.2 wt.% of NaCl, S2 - 6 wt.% of NaCl, and S3 - 11 wt.% of NaCl.

To construct the initial configuration for the systems with polymers only, as shown in Fig. 1 (top panel), a box of $12\times12\times8$ nm^3 was filled with water molecules. Then, polymer molecules were placed at the two water surfaces perpendicular to the z-direction, where there were 97 polymer molecules in sys. P97_S0 and 198 in sys. P198_S0. Next, the box with water and polymers was

centered and extended along z-direction to 24 nm and filled with pre-equilibrated heptol. The box was finally translated along z direction by 12 nm to center heptol in the simulation box. Similar steps were followed to build the initial configurations for sys. P97_S1 – P97_S3 and P198_S1 – P198_S3, except that some water molecules were replaced by NaCl to obtain different salinities, as shown in Table 1. For sys. VP97_S0 and VP198_S0, as shown in Fig. 1 (bottom panel), 198 VO-79 molecules were placed at the two water surfaces perpendicular to z-direction, followed by 97 polymer molecules inserted in sys. VP97_S0 and 198 inserted in sys. VP198_S0. The box was extended along z-direction to 24 nm, filled with pre-equilibrated heptol, and then translated along z-direction, similar to sys. P97_S0 and P198_S0. This design of the initial configurations was chosen to mimic the practical situation where polymer demulsifiers were added to the continuous phase of oil in which water droplets were stabilized by interfacially active components such as asphaltenes. Sys. VP97_S1 – VP97_S3 and VP198_S1 – VP198_S3 were obtained by replacing water molecules with NaCl, similar to sys. P97_S1 – P97_S3 and P198_S1 – P198_S3, as shown in Table 1.

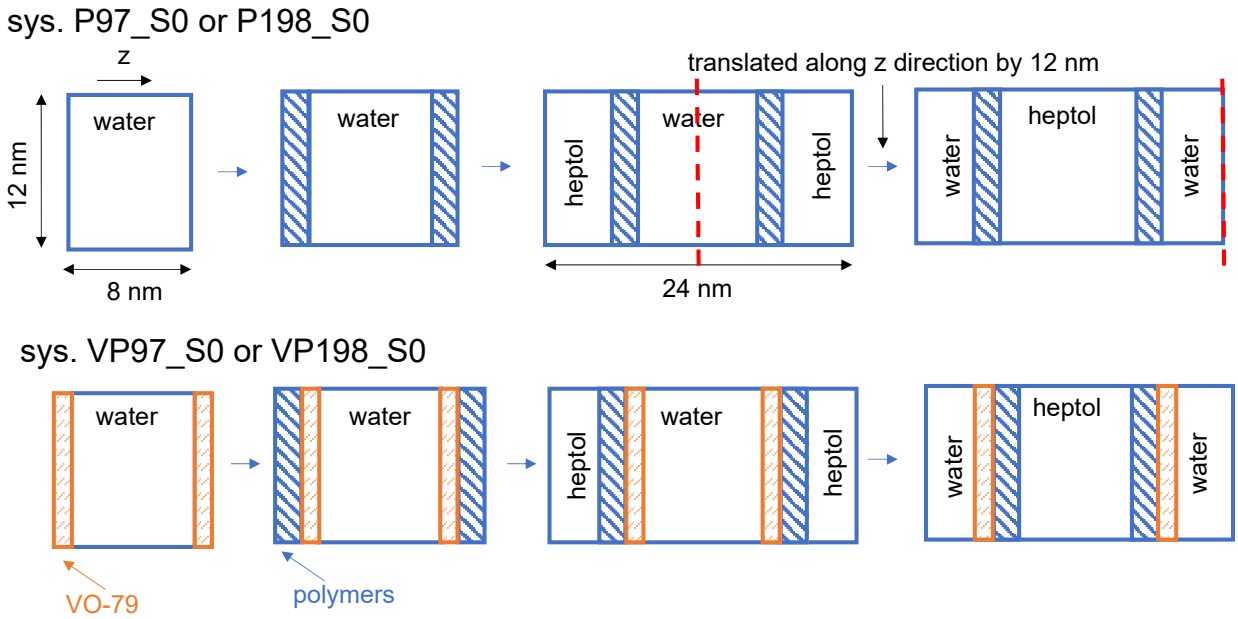

Figure 1. Schematics of building initial configurations for systems with polymer only (sys. P97_S0 or P198_S0, top) and for systems with pre-adsorbed VO-79 (sys. VP97_S0 or VP198_S0, bottom). Red dashed lines show that the center of the periodic box is translated to the edge of the box along z direction.

All MD simulations were performed using GROMACS package 5.0.7 version [34–36] with GROMOS force field parameter set 54A7. [37] The force field parameters for heptane, toluene, VO-79, and polymer have been validated in our previous work. [38] The density of organic solvents and IFT of water/organic solvent interfaces were validated as shown in SI section SI1. Water molecules were represented by the Simple Point Charge (SPC) model, which is one of the commonly used water models (SPC, SPC/E, TIP3P and TIP4P) in MD simulations of interfacial problems involving salt. [39] Each system underwent a static energy minimization, 100 ns NVT and 100 ns NPT equilibration. Then, each system was subjected to a 40 ns simulation in $NP_{normal}AT$ ensemble, where P_{normal} was the isonormal pressure perpendicular to the x-y plane (i.e., in z-direction), and A was the iso-interfacial area of the x-y plane. The v-rescaling thermostat was used to achieve constant temperature at 300 K, and Parrinello-Rahman [40] semi-isotropic pressure coupling was used to obtain constant pressure of 1 bar in z-direction. In all simulations, periodic boundary condition was applied to x, y, and z directions. LINCS [41] algorithm, full electrostatics with particle-mesh Ewald methods [42] was applied, and cut-off distance of 1.4 nm was used for van der Waals interaction. The results from the last 10 ns of the $NP_{normal}AT$ simulations were used to calculate the IFT using the following equation [43]:

$$\gamma = \frac{1}{2}\left(p_{zz} - \frac{p_{xx}+p_{yy}}{2}\right)L_z \quad (1)$$

where, p_{xx}, p_{yy}, p_{zz} are respectively the diagonal components of the pressure tensor, and L_z is the box length in z-direction. In SI section SI1, the IFT calculated from simulations were 34.5, 47.1 and 42.1 mN/m respectively for water/toluene, water/heptane and water/heptol (75/25) interfaces. The corresponding experimental data were 35.8-36.1, 50.2-51.1 and ~46 mN/m [44,45]. The close values provided validation for the force field parameters and methodology used to calculate IFT.

2.2 PMF calculation.

In order to quantify the free energy of adsorption at the brine/heptol interface, PMF was calculated for two sets of systems. Similar procedures were followed to build the initial configurations as explained in the previous section, except that there was only a single adsorbate molecule in heptol. In the first set of simulations (sys. V1_S0 – V1_S3), each system contained a single VO-79 with the concentration of NaCl in water being 0%, 1.2%, 6%, and 11% wt., respectively. The initial sizes of the water and heptol boxes were respectively 5×5×5 nm^3 and 5×5×7 nm^3. Each system in the second set of simulations (sys. P1_S0 – P1_S3) contained a single polymer molecule. The water and heptol boxes had the initial size of 10×10×10 nm^3 and 10×10×12 nm^3.

Each system underwent energy minimization, NVT (100 ps) and NPT (100 ps) equilibration, and production run (20 ns) with the same simulation parameters as described in the previous section. During the production run, the location (along z-direction) of water/heptol interface was determined by the intersection of the density profiles of water and heptol, which were recorded every 50 ps. The distance between the interface and the center of mass (COM) of the adsorbate, VO-79 or polymer, was calculated. The configuration that corresponded to the minimum distance was used as the initial configuration for steered MD (SMD) simulation. [46,47] During the SMD,

a harmonic potential (spring constant of 1000 kJ/(mol·nm^2)) was applied on the COM of the adsorbate, which was pulled along z-direction from the water/heptol interface toward the bulk heptol phase at a pulling rate of 0.01 nm/ps. For the first set of simulations with VO-79 as the adsorbate, the pull time was 300 ps and the total displacement for the COM of VO-79 was ~ 3 nm. For the second set with polymer as the adsorbate, the pull time was 600 ps and the total displacement for the COM of the polymer was ~ 6 nm.

PMF calculations were then performed with the reaction coordination (ζ) defined as the distance between the COM of the adsorbate and the location of the interface determined at the beginning of each SMD simulation. For each system (with a given adsorbate and NaCl concentration), a total of 30 configurations were extracted from SMD and used as the initial configurations for umbrella sampling (US). [48,49] During each US simulation, an external biasing potential with a spring constant of 10,000 kJ/(mol·nm^2) was applied to the COM of the adsorbate. Each system underwent a brief NPT equilibration and 2 ns US simulation using SMD at zero pull rate. Weighted histogram analysis method (WHAM) [48,50] was used to analyze the data obtained from the US simulations and generate the PMF as a function of ζ. The details of US are shown in SI section SI2.

3. Results and Discussion

3.1 Free energy of adsorption for a single adsorbate.

Free energy profiles for the adsorption of VO-79 or polymer were obtained by PMF calculations using US as described in section 2.2. Fig. 2 shows the PMF as a function of ζ, the location of the COM of the adsorbate relative to the water/heptol interface. The lowest value for ζ was obtained when the adsorbate was closest to the aqueous phase, as shown in Fig. 2a and 2d for sys. V1_S2 and P1_S2 respectively (corresponding figures for the other systems are shown in SI section SI3). The largest value of ζ corresponded to the adsorbate near the center of the heptol phase (Fig. 2b

and e). ζ could take negative values if the adsorbate was found to penetrate into the water phase. The PMF for a single VO-79 molecule (sys. V1_S0 - V1_S3) and that for a single polymer molecule (sys. P1_S0 – P1_S3) are plotted in Fig. 2c and Fig. 2f, respectively. When the adsorbate molecule was far from the interface ($\zeta \sim$ 2-3 nm in Fig. 2c and $\zeta \sim$ 4-6 nm in Fig. 2f), the PMF curve reached a plateau and the average value over the plateau was used as the reference state (state 1) where the PMF was set to zero. The minimum in each PMF curve was referred to as state 2, and the adsorption free energy was defined as the difference in PMF between states 2 and 1, ΔG_{2-1}. ΔG_{2-1} was negative in all cases, suggesting favorable adsorption at the interface. In Fig. 2c, the absolute free energy change ($|\Delta G_{2-1}|$) for sys. V_S0 (3.81 kCal/mol) was similar to that for sys. V1_S1 (3.70 kCal/mol). Sys. V1_S2 had the largest $|\Delta G_{2-1}|$ (4.32 kCal/mol) and sys. V1_S3 had the smallest (3.36 kCal/mol), while the difference in $|\Delta G_{2-1}|$ was insignificant among sys. V1_S0 – V1_S3. In Fig. 2f, $|\Delta G_{2-1}|$ was smallest in sys. P1_S0 (12.68 kCal/mol), increased in sys. P1_S1 (14.95 kCal/mol), slightly decreased in sys. P1_S2 (13.55 kCal/mol) and then increased again in sys. P1_S3 (14.77 kCal/mol).

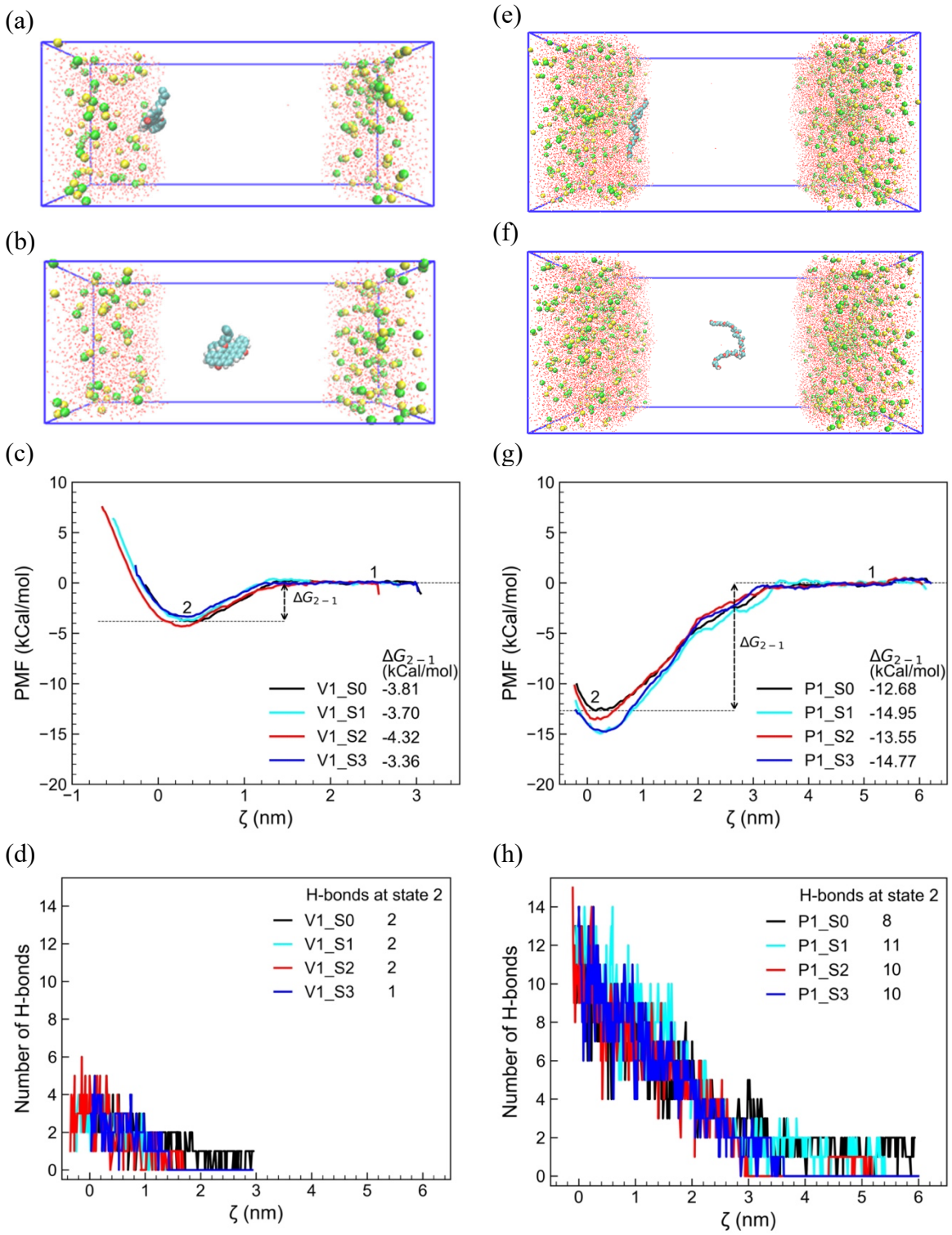

Figure 2. Snapshots of a single VO-79 molecule (sys. V1_S2) (a) located at brine /heptol interface and (b) far from the interface. Snapshots of a single polymer molecule (sys. P1_S2) (e) located at brine /heptol interface and (f) far from the interface. Red line: water; yellow: Na^+; green: Cl^-; cyan:

carbon; red: oxygen. PMF for the adsorption of (c) a single VO-79 molecule in sys. V1_S0 – V1_S3, and (g) for a single polymer molecule in sys. P1_S0 – P1_S3. Number of hydrogen bonds during SMD (d) between the single VO-79 and water molecules in sys. V1_S0 – V1_S3 and (h) between the single polymer molecule and water molecules in sys. P1_S0 – P1_S3.

The number of H-bonds between VO-79 (or polymer) and water molecules during SMD is plotted in Fig. 2d and 2h. The values at state 2 are shown along with the legend. Due to the fluctuation in each curve, this value was calculated by averaging 5 data points nearest to state 2. In Fig. 2d, at ζ where the PMF was the lowest (state 2), there were only 1-2 hydrogen bonds (H-bonds) between VO-79 and water for sys. V1_S0 – V1_S3, whereas the H-bonds between polymer and water was 4 to 10 times higher (ranging from 8 to 11 for sys. P1_S0 – P1_S3), as shown in Fig. 2h. This drastic difference led to much larger $|\Delta G_{2-1}|$ of a single polymer compared with VO-79. One of the requirements for a polymer demulsifier to be effective is that it has a higher affinity to the interface than asphaltenes and can therefore penetrate the asphaltene film. [51] The PMF data in Fig. 2c and 2g confirmed that the PEO_5-PPO_{10}-PEO_5 copolymer possessed this property. Fig. 2 also shows that the addition of NaCl had different influences on the adsorption free energy of VO-79 and the polymer: it enhanced $|\Delta G_{2-1}|$ for the polymer while having insignificant impact on $|\Delta G_{2-1}|$ for VO-79. H-bonding data in Fig. 2d and 2h agreed with this observation: when NaCl was added, the number of H-bonds between water and VO-79 at state 2 either did not change (for sys. V1_S1 and V1_S2) or decreased (for sys. V1_S3), whereas the number of H-bonds between water and the polymer increased from 8 in sys. P1_S0 to 10 or 11 in sys. P1_S1 – P1_S3. It suggests the presence of salting-in effect [52,53] in sys. P1_S1 – P1_S3 where the addition of NaCl promoted the solubility of the polymer's hydrophilic PEO blocks in the aqueous phase. In fact,

among sys. P1_S1 – P1_S3, sys. P1_S2 had the largest density of NaCl near the interface (SI section SI4), which reduced the interaction between polymer and water, and as a result its $|\Delta G_{2-1}|$ was the smallest. Contrary to the polymer, the added NaCl was unable to induce the salting-in effect for VO-79.

3.2 Molecular distributions near interfaces.

The density profiles along z direction for all components in sys. P97_S0, P198_S0, VP97_S0, VP198_S0 are plotted in Fig. 3. Each density profile was averaged over the last 10 ns of the simulation when the system reached equilibrium. For sys. P97_S0 (Fig. 3a) and P198_S0 (Fig. 3b), there were two sharp peaks for the density distribution of polymers, which were located at the water/heptol interface. As shown in the corresponding snapshots, in each system the polymers were adsorbed and formed a film on each of the two interfaces. In sys. VP97_S0 (Fig. 3c), the density profile for the polymer had two sharp peaks which were located closer to the water phase than the peaks for VO-79. With a higher concentration of polymers in sys. VP198_S0 (Fig. 3d), the density profile of polymers had two broad peaks at the water/heptol interfaces, while sharp peaks were observed for VO-79 and located within the broad peaks of the polymers. Recalling that in both sys. VP97_S0 and VP198_S0, the VO-79 molecules pre-adsorbed at the water surfaces before the polymer molecules were added next to them, the results implied that the polymers penetrated into the VO-79 film, ultimately leading to the formation of polymer/VO-79 complexes where VO-79 molecules were embedded in the polymer film. Data in SI sections SI5 confirmed that there were stronger interactions between water and polymer than between water and VO-79, also consistent with the PMF result for a single adsorbate observed in section 3.1. Density profiles for all components (except ions) in sys. P97_S1 – P97_S3, P198_S1 – P198_S3, VP97_S1 –

VP97_S3 and VP198_S1 – VP198_S3 as well as the corresponding final configurations were plotted in SI section SI6. Similar observations were obtained for the density profiles of polymers and VO-79 in these systems, indicating that qualitatively the distributions of polymers and VO-79, and the formation of a VO-79-in-polymer interfacial film structure, were not affected by the addition of NaCl.

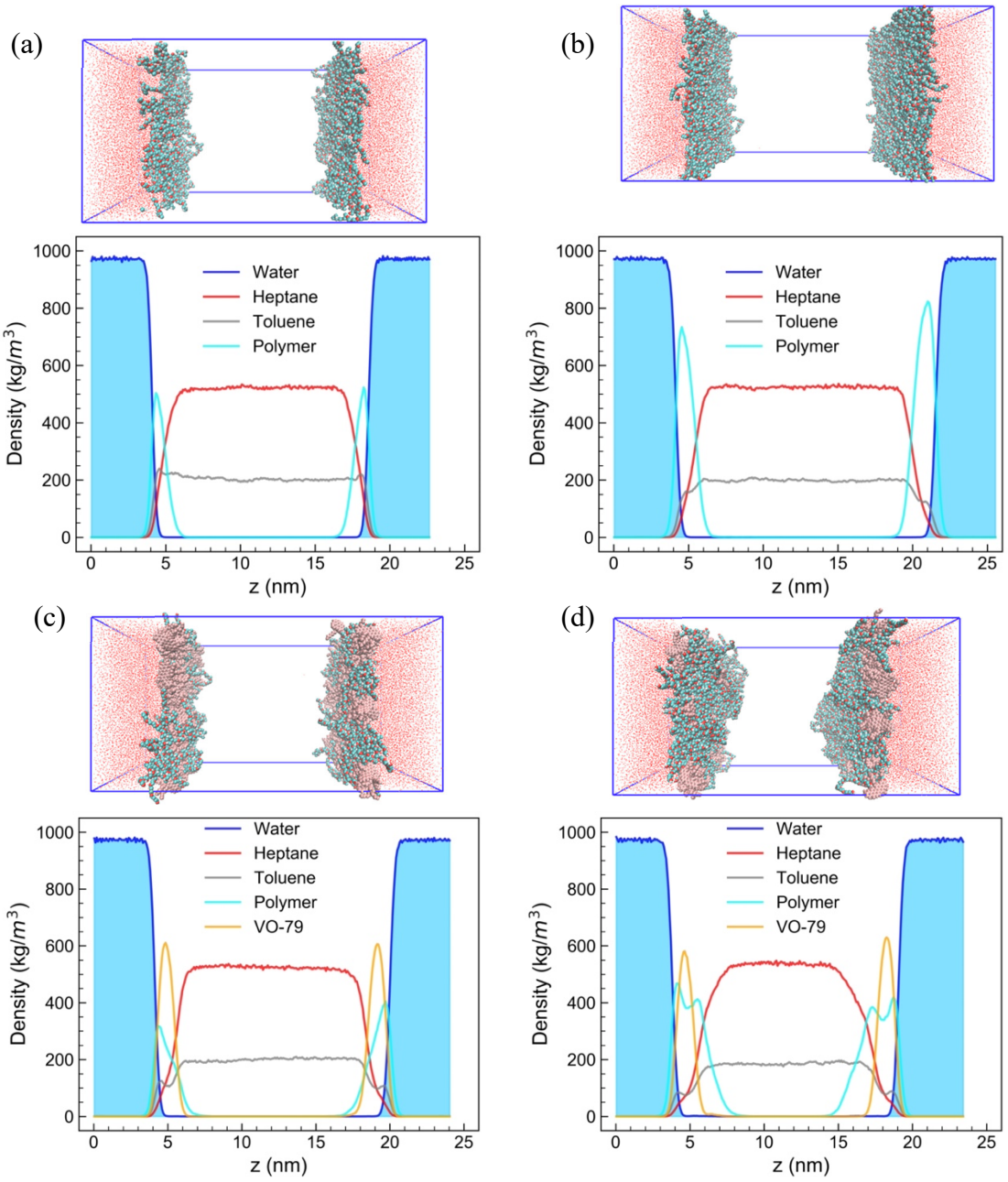

Figure 3. Snapshots of final configurations (top; red lines: water, cyan and red: carbon and oxygen atoms in polymer, pink spheres: atoms in VO-79) and density profiles (bottom) for all components in (a) sys. P97_S0, (b) sys. P198_S0, (c) sys. VP97_S0, and (d) sys. VP198_S0.

Number densities of NaCl are shown in Fig. 4a for sys. VP97_S1 – VP97_S3 and VP198_S1 - VP198_S3, and in SI section SI6 for the other systems. The two vertical dashed lines in Fig. 4a

represent the Gibbs dividing planes at the two interfaces [54] which, according to Fig. 3, exhibited symmetric nature with respect to the center of the simulation box. The surface excess of NaCl, Γ_{NaCl}^{excess}, can be obtained from the following equation [54]:

$$\Gamma_{NaCl}^{excess} = \int_{z_H}^{z_0} c_{NaCl}(z)dz + \int_{z_0}^{z_B} (c_{NaCl}(z) - c_{Nacl}^{bulk})dz \quad (2)$$

where, $c_{NaCl}(z)$ is the number density of NaCl at z and c_{NaCl}^{bulk} is the bulk number density of NaCl in the solvent (water). The Gibbs dividing plane (z_0) is defined as the location where the surface excess of water reaches zero. [54] Fig. 4b shows an example, for one of the interfaces in sys. VP97_S2, where the Gibbs dividing plane was located near z = 20 nm. The orange shaded region, to the right of z_0, has the same area as the cyan shaded region to the left of z_0. z_H in equation (2) is the location of the bulk heptol phase, in this case a few nm away to the left of the Gibbs dividing plane, and z_B is the location where the NaCl number density reaches c_{NaCl}^{bulk}. In Fig. 4b, the number density of NaCl was negligible between z_H and z_0, and gradually increased to a plateau in at z_B. Consequently, the first integral in equation (2) is negligible compared with the second integral, which is negative since c_{Nacl}^{bulk} is greater than $c_{NaCl}(z)$ from z_0 to z_B. Defining c_{Nacl}^{bulk} from the average of $c_{NaCl}(z)$ at five largest z (> z_B) values, Γ_{NaCl}^{excess} for the interface near z = 20 nm in sys. VP97_S2 was calculated to be -0.93 μmol/m^2. Γ_{NaCl}^{excess} for the interface near z = 5 nm (Fig. 4a top middle) can be similarly calculated, with a change in the direction of integration (going towards left from bulk heptol in the middle to bulk water located on the left).

Fig. 4c summarizes the Γ_{NaCl}^{excess} values, which were negative for all systems. For the same system, Γ_{NaCl}^{excess} on the two interfaces exhibited some differences, as the distributions of molecules around them were not identical. There were also limitations associated with the calculations for systems that had the highest salinity, since the number density in bulk water was non-uniform (see Fig. 4a, right panels). As a result, c_{Nacl}^{bulk} was difficult to define, although in our calculations we still

used the average of $c_{NaCl}(z)$ at five largest z values (for the right interface) and at five lowest z values (for the left interface), for the sake of consistency. Nevertheless, a clear trend could be observed as the NaCl concentration increased: with the same type and concentration of adsorbates, higher NaCl concentration led to larger $|\Gamma_{NaCl}^{excess}|$.

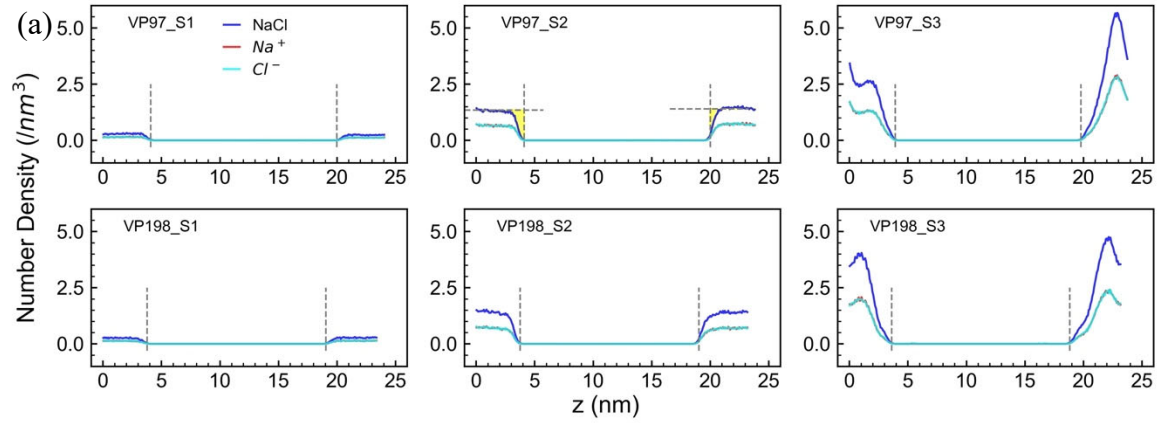

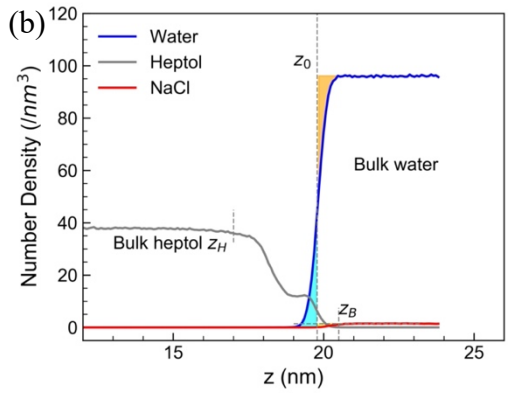

(c) Surface excess of NaCl (μmol/m^2)

Sys.	VP97_	VP198_	P97_	P198_
S1	-0.09 -0.19	-0.20 -0.26	-0.19 -0.21	-0.17 -0.20
S2	-1.44 -0.93	-1.61 -1.51	-0.48 -0.86	-1.05 -1.05
S3	-5.07 -11.2	-8.45 -9.88	-13.3 -15.9	-12.7 -10.0

Figure 4. (a) Number density profiles of NaCl for sys. VP97_S1 – VP97_S3 and VP198_S1 – VP198_S3 (yellow regions shown in sys. VP97_S2 are the surface excess); (b) Illustration of Gibbs dividing plane (z_0) and calculation of surface excess in sys. VP97_S2; and (c) Table of Γ_{NaCl}^{excess} (in μmol/m^2) for all studied systems; two values in each system are for the two interfaces.

Negative Γ_{NaCl}^{excess} values in Fig. 4c confirmed that NaCl was depleted from the interface and dissolved in bulk water. With Na^+ and Cl^- ions in the aqueous phase, the water molecules form a cage-like hydration shell around the ions. [55,56] Water near an interface is exposed to another

phase so that the hydration shells for ions are disrupted, resulting in the tendency of ions being depleted from the interface. [55] In addition, Fig. 4a shows that at very high salinity, the distribution of NaCl in bulk water was non-uniform and even had a prominent peak in the case of 11 wt.% NaCl, suggesting the possibility of salt ion aggregation [57–59]. To examine this, radial distribution function (RDF) for the COM of water molecules with respect to Na^+ and Cl^- ions are plotted in Fig. 5a for control sys. C_S1 – C_S3 and in Fig. 5b for sys. VP198_S1 – VP198_S3. As shown in Fig. 5a, the RDF curve had its first prominent peak located at ~ 0.25 nm and the first minimum at ~0.28 nm. The number of water molecules within the first hydration shell (N_{HS}) was quantified by the cumulative number where the RDF curve reached the minimum, and the values are shown in each subfigure. N_{HS} decreased slightly from sys. C_S1 to C_S2 and decreased drastically from sys. C_S2 to C_S3. With higher NaCl concentration in sys. C_S2 than in sys. C_S1, there was higher probability for salt ions to associate instead of being solvated by water, causing a small reduction in N_{HS}. The aggregation of salt ions was more pronounced in sys. C_S3, as shown in SI section SI6, and N_{HS} decreased significantly. A similar trend was observed for sys. VP198_S1 – V198_S3 (Fig. 5b) and the other systems (SI section SI7). Additionally, N_{HS} in sys. P97_S3, P97_S3, VP97_S3 and VP97_S3 ranged from 0.93 to 0.96, which was lower than the value (1.57) for the corresponding control system C_S3 without adsorbates, indicating that the aggregation of salt ions was more pronounced in the systems with adsorbates. A plausible explanation is that with the adsorbates, the water molecules tended to interact with the adsorbates at the interface, thus less water was available to form hydration shells for the salt ions. Interestingly, the PMF results for a single polymer suggested that the addition of NaCl was associated with enhanced polymer/water interaction (increased $|\Delta G_{2-1}|$), which was in line with the reduced ion hydration observed here.

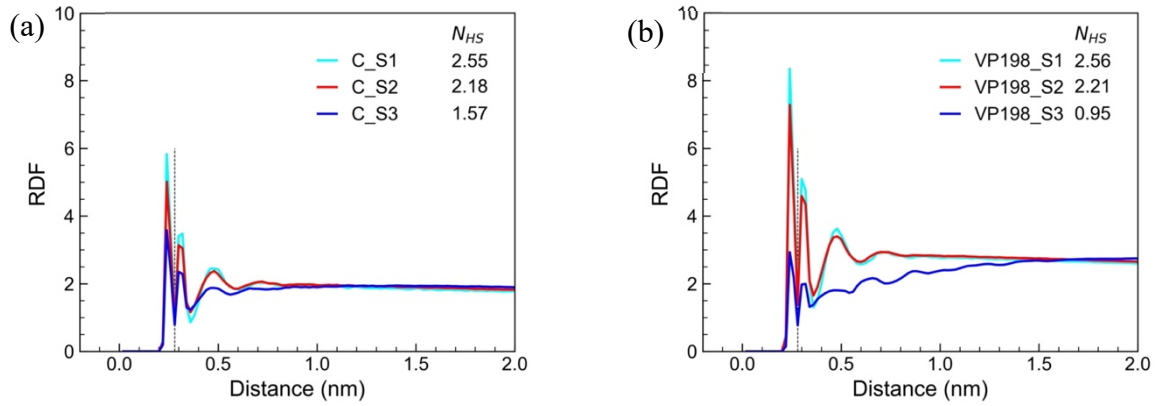

Figure 5. RDF for the COM of water molecules with respect to Na^+ and Cl^- ions, averaged over the last 5 ns of simulation, for (a) sys. C_S1 – C_S3 and (b) sys. VP198_S1 – VP198_S3. The radius of the first hydration shell was defined as the location of the first minimum in each RDF curve, marked by dashed black line. Cumulative number of water molecules in the first hydration shell (N_{HS}) is shown along with the legend for each system.

3.3 Interfacial tension.

Water/heptol IFT for all simulated systems are summarized in Fig. 6. Data was collected every 1 ns during the last 10 ns of the NP_nAT simulations, and the averages are shown as symbols with their standard deviations indicated by error bars. Data for the control systems without adsorbates (sys. C_S0-C_S3) were clearly above those for the other systems, indicating that the adsorption of surface-active components resulted in a decrease in IFT. Similar reduction was reported experimentally and theoretically for water/toluene interface. Specifically, the water/toluene IFT was in the range of 35.8-36.1 mN/m [44], while the value decreased to 12.0-13.1 mN/m with the addition of 200 ppm Poloxamer 181 (a PEO_x-PPO_y-PEO_z polymer) [60]. In addition, at the same NaCl concentration, Fig. 6 shows that higher concentration of a given type of adsorbates caused greater reduction in IFT (e.g., P198_S0 vs. P97_S0, VP198_S1 vs. VP97_S1). In the absence of adsorbates (sys. C_S0-C_S3), the IFT increased slightly when NaCl concentration increased from

0 to 1.2 wt.%, rose more evidently as NaCl concentration increased to 6 wt.%, and then slightly decreased at 11 wt.% NaCl concentration. The effect of NaCl concentration on the IFT followed the similar trend for sys. P97_S0 – P97_S3 and sys. P198_S0 – P198_S3. For systems with both VO-79 and polymers, the IFT increased when NaCl concentration increased from 0 to 1.2 wt.%, and then decreased with further increase of NaCl concentration up to 11 wt.%.

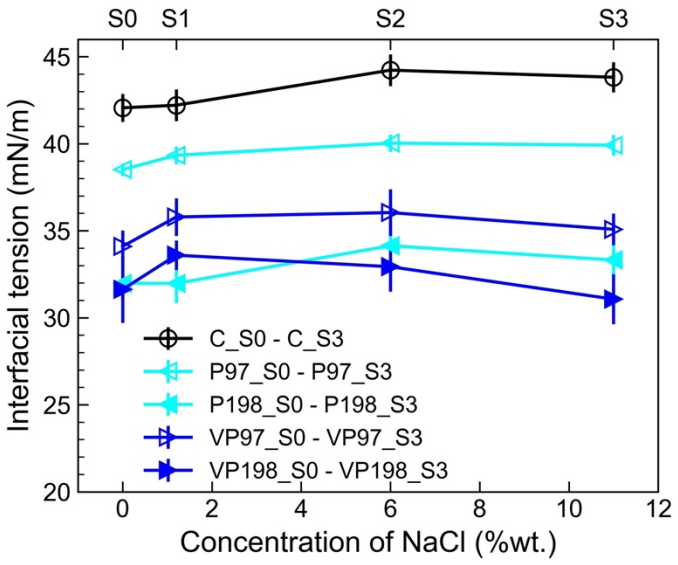

Figure 6. Interfacial tension of water/heptol interfaces vs. the concentration of NaCl.

According to the Gibbs adsorption isotherm [61], the difference in interfacial tension $d\gamma$, between a pure water/oil interface and the interface with surfactants, is a function of the bulk concentration of surface-active species in the solution, C_i, given by the following equation:

$$d\gamma = -RT \sum \Gamma_i \, d\ln C_i \tag{3}$$

where, R is the gas constant, T is the absolute temperature, Γ_i is the equilibrium surface excess for component i; the summation taken over all the solutes in the solution. As discussed in Fig. 4, Na^+ and Cl^- ions were depleted from the interface and $\Gamma_{NaCl}^{excess} < 0$, so that the water/heptol IFT

increased upon increasing NaCl concentration ($d\ln C_{NaCl} > 0$) from 0 to 6 wt.% in the control systems (C_S0 – C_S2) as shown in Fig. 6. The increasing trend of IFT upon increasing salt concentration has been reported in many studies that incorporated pure hydrocarbon as the oil phase. [8,62] Our results for NaCl concentration up to 6 wt.% were consistent with these previous reports. However, in this work the IFT in sys. C_S3 with 11 wt.% of NaCl was similar to sys. C_S2, which was attributed to salt aggregation in highly concentrated solutions. In fact, the linear correlation between $d\gamma$ and $d\ln C$ as stated by the Gibbs adsorption isotherm (equation 3) is only applicable when the concentration C is below a critical micelle concentration of a surfactant [63]. When C was sufficiently high, γ was reported to remain almost constant as C increased [63]. Consistently, in this work, the IFT did not show an evident change when the NaCl concentration increased from 6 wt.% in sys. C_S2 to 11 wt.% in sys. C_S3.

As shown in Fig. 3, the polymers adsorbed at the interface and their bulk concentrations in both heptol and aqueous phases was negligible. Performing a calculation analogous to equation (2), the surface excess of polymer, $\Gamma_{polymer}^{excess}$, was 1.12 μmol/m^2 for systems with 97 polymer molecules (sys. P97_S0 – P97_S3 and sys. VP97_S0 – VP97_S3) and 2.28 μmol/m^2 for systems with 198 polymer molecules (sys. P198_S0 – P198_S3 and sys. VP198_S0 – VP198_S3). $\Gamma_{polymer}^{excess}$ was insensitive to NaCl concentration because in all systems the polymers were fully adsorbed. The positive $\Gamma_{polymer}^{excess}$ suggested that increasing the polymer concentration ($d\ln C_{polymer} > 0$) would result in the reduction of IFT, which was confirmed by Fig. 6. In addition, similar to sys. C_S0 – C_S3, the IFT for sys. P97_S0 – P97_S3 and P198_S0 – P198_S3 followed a non-monotonic trend as the NaCl concentration increased. With ionic surfactants present in the system, a previous study stated that increasing the salt concentration could cause the reduction of IFT, due to the interaction between ionic surfactants and salt ions at the interface. [55] On the contrary, with non-ionic

surfactants, IFT of toluene/brine was reported to increase when the NaCl concentration increased from 0 to 15 wt.%. [55] The first prominent peak in the RDF of NaCl ions with respect to the polymer (SI section SI8) implied the existence of interaction between ions and polymers, but the intensity was much lower than that between water and polymer (SI section SI5). The polymer/water interaction was therefore facilitated by NaCl ions not through polymer/ion interaction, but through the ion depletion from the interface. Jian et al. reported that the reduction in the IFT of water/toluene interface upon the addition of interfacial-active molecules was correlated to the H-bonds formed at the interface. [27] The number of H-bonds between polymers and water (Fig. 7a) had a negligible difference among sys. P97_S0 – P97_S3 and among sys. P198_S0 – P198_S3. This was different from the case of single polymer adsorption, where the salting-in effect increased the solubility of hydrophilic PEO blocks in the polymer and its H-bonds with water (discussed in Fig. 2h). The same phenomenon not observed when a polymer film was formed, restraining the mobility of individual chains. Since the concentration of the polymer was constant among sys. P97_S0 – P97_S3 (and among sys. P198_S0 – P198_S3), the contribution of $d\ln C_{polymer}$ to $d\gamma$ in equation 3 was expected to be similar. The difference in $d\gamma$ was therefore caused mainly by $d\ln C_{NaCl}$, resulting in the same IFT trend in sys. P97_S0 – P97_S3 (and sys. P198_S0 – P198_S3) as compared to the control systems. The role of polymer here was to cause an overall reduction of the IFT compared to sys. C_S0 – C_S3.

With the co-adsorption of VO-79 and polymers, the IFT curve for sys. VP97_S0 – VP97_S3 was further lowered compared with sys. P97_S0 – P97_S3 containing solely the polymers. The surface excess of VO-79, Γ_{VO-79}^{excess}, was calculated to be 2.17 μmol/m^2 for sys. VP97_S0 – VP97_S3. This positive value was consistent with the reduction in γ brought by VO-79, which was also observed in the literature upon the increase of asphaltene concentration. [12,64] The total number

of H-bonds between adsorbates and water slightly increased from sys. P97_S0 – P97_S3 (Fig. 7a) to sys. VP97_S0 - VP97_S3 (Fig. 7b), which agreed with the finding of Jian et al. that the increase of H-bond led to the lowering of IFT. [27] In sys. VP97_S0 – VP97_S3, there were two types of adsorbates (97 polymers and 188 VO-79 molecules), and they had different contributions to H-bond formation with water. The number of H-bonds was in the range of 179-188 between VO-79 and water, and 612-632 between polymer and water. The snapshots and density profiles (Fig. 3 and SI section SI6) suggested that the interfacial film possessed a structure where the VO-79 molecules and their aggregates (see SI section SI9 for VO-79 aggregation data) were embedded in the polymer network, as shown schematically in Fig. 7c. Such a structure facilitated H-bond formation by the polymers while limiting H-bond formation by VO-79. As a result, although aggregation of asphaltenes was reported to impact water/toluene IFT [28], evident correlation between aggregate size of VO-79 and IFT was not found in this work (see SI section SI9). One should not, however, neglect the relatively small amount of H-bonds formed by VO-79 with water. As seen in Fig. 2d and 2h, the number of H-bonds between a single polymer and water was 4-10 times that between a single VO-79 and water, while the magnitude of the adsorption free energy had only 3.1-4.4 times difference. It indicated that the adsorption free energy was more sensitive to the change in the number of VO-79/water H-bonds. From sys. VP97_S0 to VP97_S1, the number of VO-79/water H-bonds decreased from 188 to 179, while the number of polymer/water H-bonds increased from 623 to 632. The evident increase of IFT in VP97_S1 was attributed to the reduction of VO-79/water H-bonds and increase in $\ln C_{NaCl}$. From sys. VP97_S1 to VP97_S2, the number of VO-79/water H-bonds slightly increased to 183, while the number of polymer/water H-bonds decreased to 612. The former tended to decrease the IFT while the latter, along with the increase in $\ln C_{NaCl}$, tended to increase the IFT. In Fig. 6, the average IFT showed a small decrease

from sys. VP97_S1 to VP97_S2, but the change was within the standard deviation. The decrease in IFT from sys. VP97_S2 to VP97_S3 was consistent with the increase in the number of both VO-79/water and polymer/water H-bonds.

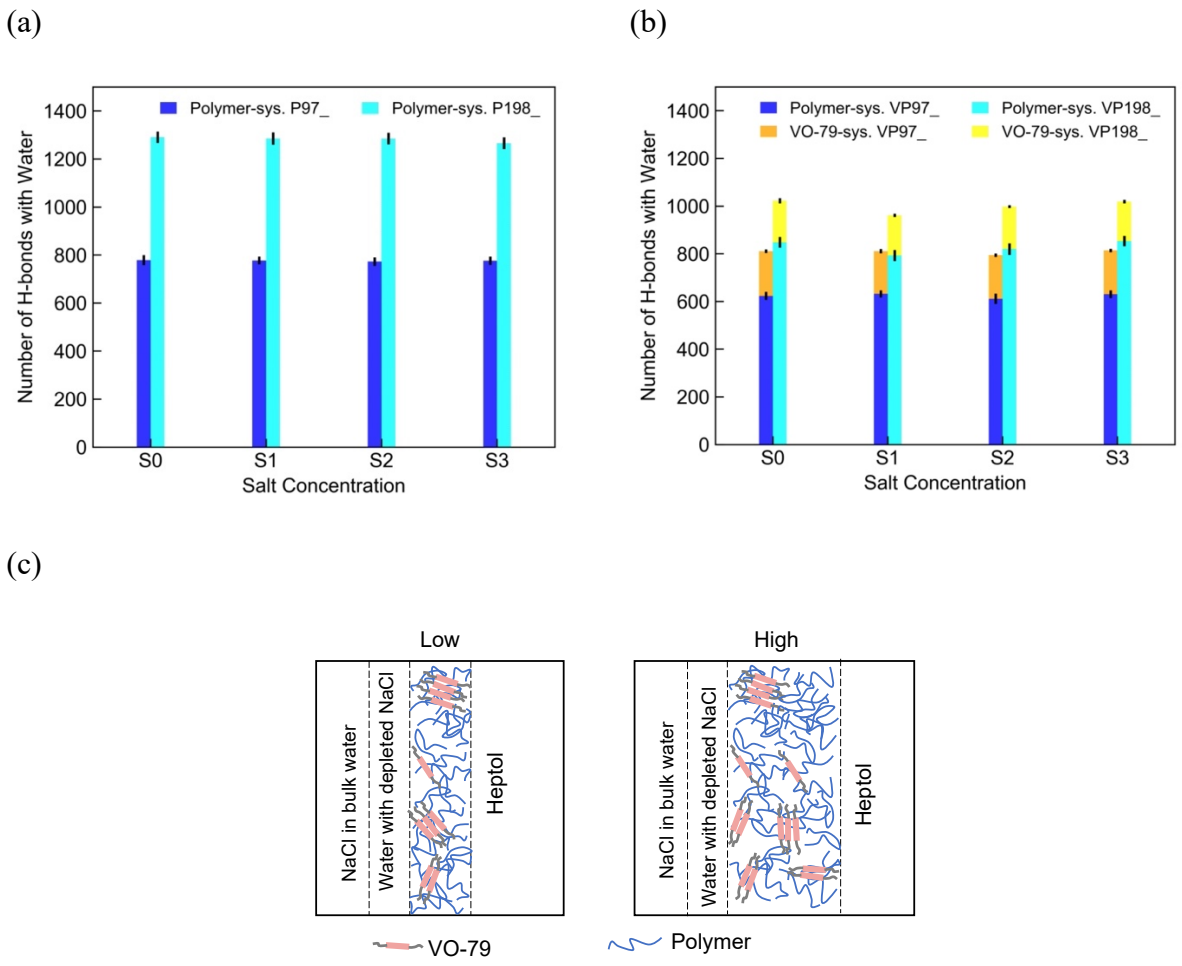

Figure 7. (a) Number of H-bonds between water and polymer in sys. P97_S1 – P97_S3 (blue) and sys. P198_S1 – P198_S3 (cyan); (b) Number of H-bonds between water and polymer (blue), and between water and VO-79 (orange) in sys. VP97_S - VP97_S3. Number of H-bonds between water and polymer (cyan), and between water and VO-79 (yellow) in sys. VP198_S0 – VP198_S3; (c) Schematics of interfacial films with low (left) and high (right) concentrations of polymers.

For sys. VP198_S0 – VP198_S3, the number of H-bonds between polymer and water (793-853) was significantly higher and varied more evidently than that between VO-79 and water (165-178), as shown in Fig. 7b. Compared with sys. VP97_S0 – VP97_S3 where the number of VO-79/water H-bonds was in the range of 179-188, the increased amount of polymers provided stronger shielding for the interaction of VO-79 with water. The change in IFT was therefore mainly influenced by the polymer/water interaction. In fact, the IFT for sys. VP198_S0-VP198_S3, as shown in Fig. 6, was reversely correlated to the number of polymer/water H-bonds (Fig. 7b). It is also interesting to see from Fig. 7 that less H-bonds were formed between water and the adsorbates in sys. VP198_S0 – VP198_S3 as compared to sys. P198_S0 – P198_S3, although the former set of systems contained 188 VO-79 molecules in addition to the same number of polymers. The complexation of polymer with VO-79 at the interface not only restricted the access of VO-79 to water, but also reduced the interaction of water with the adsorbates as a whole. Overall, with both polymer and VO-79 at the interface, the non-monotonic effect of salinity on IFT remained, but the transition occurred at a lower concentration compared with systems not containing VO-79.

Change in IFT is often accompanied by redistribution of charges in the interfacial region [65]. Fig. 8 examines the charge density distribution for individual components and their sum near one of the interfaces, around z = 5 nm. For all the systems, the total charge density exhibited a negative peak on the left (further from the oil phase) and a positive peak on the right (closer to the oil phase), separated by a distance of ~ 2 nm. These two peaks coincided with the corresponding peaks for the charge distribution of water, suggesting that the orientation of water molecules was a major source of the induced interfacial polarity. In addition, in the systems with only polymers (first two rows in Fig. 8), the two curves for water and the entire system almost overlapped, indicating that water orientation played a dominant role. With both VO-79 and polymers at the interface (last two

rows in Fig. 8), the two curves for water and the entire system showed deviations. While the charge distribution of water still had one negative peak and one positive peak, a second positive peak appeared in the charge density of the entire system (closer to the oil phase). As well, the first positive peak (at around z = 4.5 nm) was noticeably lower than the peak in the water charge density distribution. Both changes correlated with the charge density distribution of VO-79, and hence VO-79 contributed to reducing the interfacial polarity. The effect of NaCl on the interfacial polarity was subtle: the charge density curves for NaCl exhibited multiple peaks with no clear correlation with the total charge density distribution. It is more likely that the influence of NaCl was manifested through the charge distribution of water, since surface depletion of NaCl and aggregation of the salt ions both impacted the water structure.

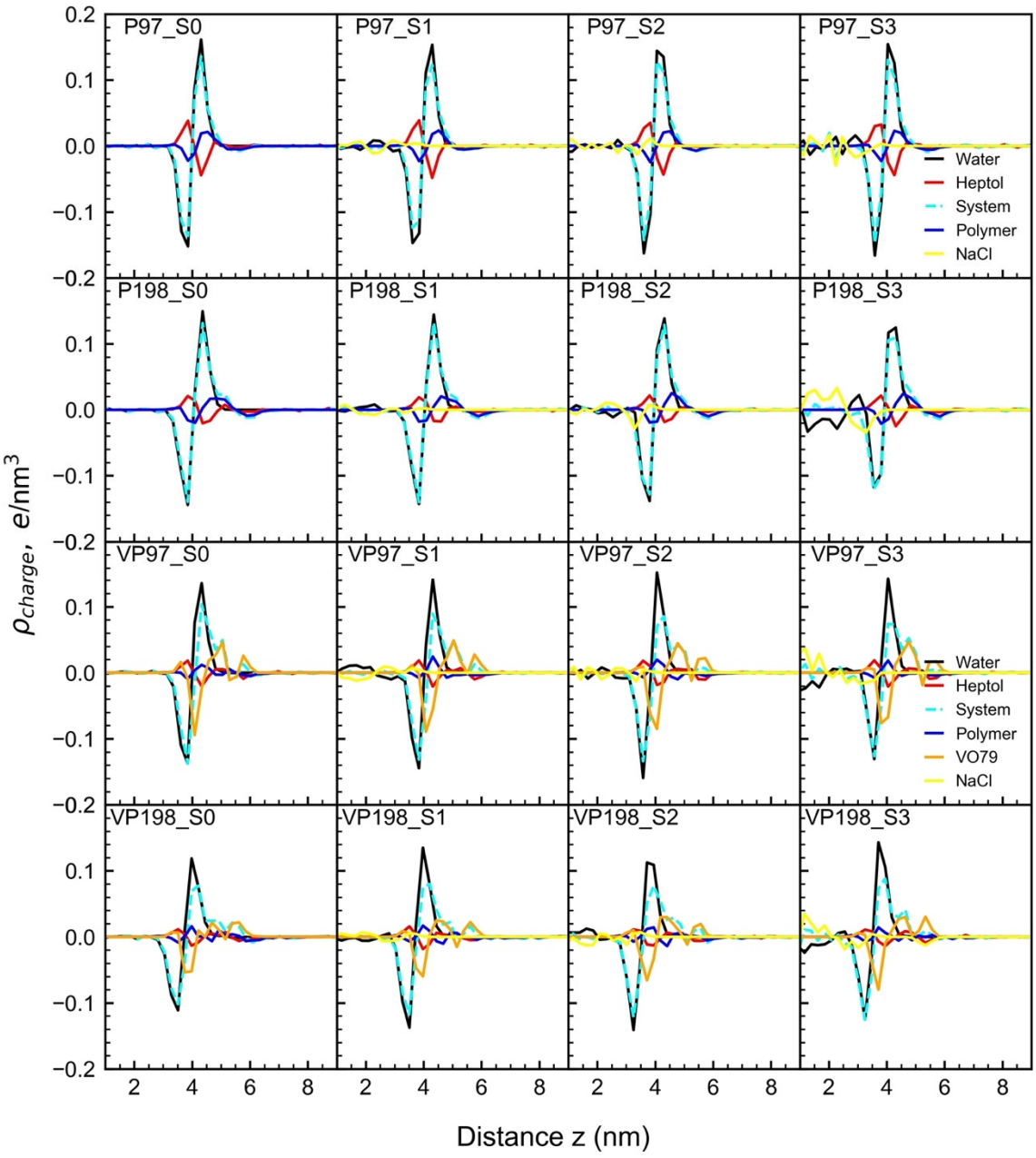

Figure 8. Charge distribution along z direction for the interface near z = 5 nm. Left to right: sys. P97_S0 – P97_S3 (first row), sys. P198_S0 – P198_S3 (second row), VP97_S0 – VP97_S3 (third row), and sys. VP198_S0 – VP198_S3 (fourth row).

This work showed a non-monotonic, first increasing and then decreasing, trend for the effect of NaCl concentration on the IFT at water/heptol interface. Previous studies have reported that the IFT of water/asphaltene-in-pentol interface, [13] water/asphaltene-in-toluene interface [27] and water/crude oil interface [66] increased with increasing salt concentration. This work reached a partial agreement with the statement that NaCl ions tended to have negative surface excess that resulted in the increase of IFT. Highly concentrated NaCl, however, resulted in salt ion aggregation and IFT reduction. It was also proposed in the literature that some surface-active species tended to interact with the salt ions; consequently increasing salinity might enhance the interfacial accumulation of surface-active species in oil and reduce the IFT. [7] In this work, NaCl ions, which were depleted from the interface, had negligible interactions with VO-79 and limited interaction with polymer molecules. In fact, in the absence of VO-79 the IFT change was largely dependent on the negative surface excess of NaCl when the concentration of polymer was kept constant (sys. P97_S0 - P97_S3 or sys. P198_S0 - P198_S3). Consistently, the H-bond formation in sys. P97_S0 - P97_S3 and sys. P198_S0 - P198_S3 had insignificant difference at different NaCl concentrations, and the charge distributions in these systems were almost solely dependent on the water orientation. With the presence of VO-79 and formation of VO-79/polymer complexes on the interface, the IFT was under the mutual effect of interfacial behaviors of both types of adsorbates. Firstly, the orientation or charge distribution of VO-79 counteracted with the charge distribution of water, reducing the interfacial polarity. Secondly, IFT was correlated negatively with the number of H-bonds between the adsorbates and water: the IFT was more sensitive to the change in VO-79/water H-bonds in sys. VP97_S0 - VP97_S3, but highly dependent on the polymer/water H-bonds in sys. VP198_S0 - VP198_S3 when the VO-79/water interaction was further shielded by the polymers.

It is commonly accepted that surface-active components can adsorb at the oil/water interface and reduce the IFT, which stabilizes the interface. [28] Adding low concentration of NaCl may increase the IFT of the interface with polymer or with polymer/VO-79 complexes, which would be beneficial for the destabilization of water/oil emulsion. It should be noted, however, that IFT was not the only indicator for the stability of the interface, and other factors could also play a role, such as the interfacial viscoelasticity [67]. Finally, as pointed out in the Introduction, different salt types may have different effects on the stability of oil/water interface. While NaCl was studied in this work, effect of other salt type should be further explored.

4. Conclusion

Molecular dynamics simulations were performed to investigate the effect of salinity on the stability of water/heptol interface with adsorbed polycyclic aromatic compound (VO-79) and non-ionic surfactant (PEO_5-PPO_{10}-PEO_5). The adsorption free energy of single VO-79 and polymer were quantified by the potential of mean force calculations. By introducing NaCl to the aqueous phase, the magnitude of the adsorption free energy for VO-79 had an insignificant change and that for polymer was enhanced. The interfacial tension (IFT) at water/heptol interface was calculated and correlated to the negative surface excess of salt ions and the adhesion of VO-79/polymer complex. The IFT at water/heptol interface increased when NaCl concentration increased from 0 to 6 wt.%, then slightly decreased as the concentration further increased to 11 wt.%. This non-monotonic trend was observed when there were no adsorbates, or with only polymers adsorbed. With the formation of VO-79/polymer complex, the IFT trend changed from increasing to decreasing at a lower, 1.2 wt.%, NaCl concentration, which was caused by the mutual effects of VO-79/water and polymer/water H-bonds, as well as the surface excess of NaCl.

Acknowledgment

The authors gratefully acknowledge the computing resources and technical support from the Western Canada Research Grid (WestGrid), and the financial support from the Natural Sciences and Engineering Research Council of Canada (NSERC), Syncrude Canada Ltd., Suncor Energy, Canadian Natural Resources Limited, ChampionX, the Canada Research Chairs Program, and the Future Energy Systems under the Canada First Research Excellence Fund.

Supporting information

Comparison between MD and experiments on density and IFT (SI1); Details of umbrella sampling (SI2); Initial configurations of SMD for sys. V0, V1, and V3 (SI3); Number density of NaCl in sys. P1_S1 – P1_S3 (SI4); RDF between water and adsorbates (SI5); Density profiles and final configurations (SI6); Additional RDF between water and salt ions (SI7); RDF between salt and polymer (SI8); Aggregate size of VO-79 (SI9).

Reference

[1] He L, Lin F, Li X, Sui H, Xu Z. Interfacial sciences in unconventional petroleum production: from fundamentals to applications. Chem Soc Rev 2015;44:5446–94. https://doi.org/10.1039/C5CS00102A.

[2] Alicke A, Simon S, Sjöblom J, Vermant J. Assessing the Interfacial Activity of Insoluble Asphaltene Layers: Interfacial Rheology versus Interfacial Tension. Langmuir 2020;36:14942–59. https://doi.org/10.1021/acs.langmuir.0c02234.

[3] Kirch A, Celaschi YM, de Almeida JM, Miranda CR. Brine–Oil Interfacial Tension Modeling: Assessment of Machine Learning Techniques Combined with Molecular Dynamics. ACS Appl Mater Interfaces 2020;12:15837–43. https://doi.org/10.1021/acsami.9b22189.

[4] Tang G-Q, Morrow NR. Influence of brine composition and fines migration on crude oilrbrinerrock interactions and oil recovery. J Pet Sci Eng 1999;24:91–111.

[5] Rostami P, Mehraban MF, Sharifi M, Dejam M, Ayatollahi S. Effect of water salinity on oil/brine interfacial behaviour during low salinity waterflooding: A mechanistic study. Petroleum 2019;5:367–74. https://doi.org/10.1016/j.petlm.2019.03.005.

[6] Kar T, Cho H, Firoozabadi A. Assessment of low salinity waterflooding in carbonate cores: Interfacial viscoelasticity and tuning process efficiency by use of non-ionic surfactant. J Colloid Interface Sci 2022;607:125–33. https://doi.org/10.1016/j.jcis.2021.08.028.

[7] Rocha JA, Baydak EN, Yarranton HW, Sztukowski DM, Ali-Marcano V, Gong L, et al. Role of Aqueous Phase Chemistry, Interfacial Film Properties, and Surface Coverage in Stabilizing Water-in-Bitumen Emulsions. Energy Fuels 2016;30:5240–52. https://doi.org/10.1021/acs.energyfuels.6b00114.

[8] Sauerer B, Al-Hamad M, Ma SM, Abdallah W. Effect of formation water salinity on interfacial tension of reservoir fluids. J Pet Sci Eng 2021;204:108700. https://doi.org/10.1016/j.petrol.2021.108700.

[9] Kakati A, Sangwai JS. Effect of monovalent and divalent salts on the interfacial tension of pure hydrocarbon-brine systems relevant for low salinity water flooding. J Pet Sci Eng 2017;157:1106–14. https://doi.org/10.1016/j.petrol.2017.08.017.

[10] Freer EM, Radke CJ. Relaxation of Asphaltenes at the Toluene/Water Interface: Diffusion Exchange and Surface Rearrangement. J Adhes 2004;80:481–96. https://doi.org/10.1080/00218460490477143.

[11] Jeribi M, Almir-Assad B, Langevin D, Henaut I, Argillier JF. Adsorption Kinetics of Asphaltenes at Liquid Interfaces. J Colloid Interface Sci 2002;256:268–72. https://doi.org/10.1006/jcis.2002.8660.

[12] Zhang S, Zhang L, Lu X, Shi C, Tang T, Wang X, et al. Adsorption kinetics of asphaltenes at oil/water interface: Effects of concentration and temperature. Fuel 2018;212:387–94. https://doi.org/10.1016/j.fuel.2017.10.051.

[13] Xie L, Lu Q, Tan X, Liu Q, Tang T, Zeng H. Interfacial behavior and interaction mechanism of pentol/water interface stabilized with asphaltenes. J Colloid Interface Sci 2019;553:341–9. https://doi.org/10.1016/j.jcis.2019.06.035.

[14] Ling NNA, Haber A, Graham BF, Aman ZM, May EF, Fridjonsson EO, et al. Quantifying the Effect of Salinity on Oilfield Water-in-Oil Emulsion Stability. Energy Fuels 2018;32:10042–9. https://doi.org/10.1021/acs.energyfuels.8b02143.

[15] Alves DR, Carneiro JSA, Oliveira IF, Façanha F, Santos AF, Dariva C, et al. Influence of the salinity on the interfacial properties of a Brazilian crude oil–brine systems. Fuel 2014;118:21–6. https://doi.org/10.1016/j.fuel.2013.10.057.
[16] Lashkarbolooki M, Ayatollahi S, Riazi M. Effect of Salinity, Resin, and Asphaltene on the Surface Properties of Acidic Crude Oil/Smart Water/Rock System. Energy Fuels 2014;28:6820–9. https://doi.org/10.1021/ef5015692.
[17] Moeini F, Hemmati-Sarapardeh A, Ghazanfari M-H, Masihi M, Ayatollahi S. Toward Mechanistic Understanding of Heavy Crude Oil/Brine Interfacial Tension: The Roles of Salinity, Temperature and Pressure. Fluid Phase Equilibria 2014;375:191–200. https://doi.org/10.1016/j.fluid.2014.04.017.
[18] Chávez-Miyauchi TE, Firoozabadi A, Fuller GG. Nonmonotonic Elasticity of the Crude Oil–Brine Interface in Relation to Improved Oil Recovery. Langmuir 2016;32:2192–8. https://doi.org/10.1021/acs.langmuir.5b04354.
[19] Rezaei N, Firoozabadi A. Macro- and Microscale Waterflooding Performances of Crudes which form w/o Emulsions upon Mixing with Brines. Energy Fuels 2014;28:2092–103. https://doi.org/10.1021/ef402223d.
[20] Zaki NN, Abdel-Raouf ME, Abdel-Azim A-AA. Propylene oxide-ethylene oxide block copolymers as demulsifiers for water-in-oil emulsions, II. Effects of temperature, salinity,pH-value, and solvents on the demulsification efficiency. Monatshefte Für Chem - Chem Mon 1996;127:1239–45. https://doi.org/10.1007/BF00807790.
[21] Borges B, Rondón M, Sereno O, Asuaje J. Breaking of Water-in-Crude-Oil Emulsions. 3. Influence of Salinity and Water−Oil Ratio on Demulsifier Action. Energy Fuels 2009;23:1568–74. https://doi.org/10.1021/ef8008822.
[22] Mikami Y, Liang Y, Matsuoka T, Boek ES. Molecular Dynamics Simulations of Asphaltenes at the Oil–Water Interface: From Nanoaggregation to Thin-Film Formation. Energy Fuels 2013;27:1838–45. https://doi.org/10.1021/ef301610q.
[23] Liu J, Zhao Y, Ren S. Molecular Dynamics Simulation of Self-Aggregation of Asphaltenes at an Oil/Water Interface: Formation and Destruction of the Asphaltene Protective Film. Energy Fuels 2015;29:1233–42. https://doi.org/10.1021/ef5019737.
[24] Kuznicki T, Masliyah JH, Bhattacharjee S. Aggregation and Partitioning of Model Asphaltenes at Toluene−Water Interfaces: Molecular Dynamics Simulations. Energy Fuels 2009;23:5027–35. https://doi.org/10.1021/ef9004576.
[25] Teklebrhan RB, Ge L, Bhattacharjee S, Xu Z, Sjöblom J. Initial Partition and Aggregation of Uncharged Polyaromatic Molecules at the Oil–Water Interface: A Molecular Dynamics Simulation Study. J Phys Chem B 2014;118:1040–51. https://doi.org/10.1021/jp407363p.
[26] Alhosani M, Asthagiri D, Puerto M, Chapman WG. Insights into the mechanisms affecting water/oil interfacial tension as a function of salt types and concentrations. Fluid Phase Equilibria 2020;522:112771. https://doi.org/10.1016/j.fluid.2020.112771.
[27] Jian C, Poopari MR, Liu Q, Zerpa N, Zeng H, Tang T. Mechanistic Understanding of the Effect of Temperature and Salinity on the Water/Toluene Interfacial Tension. Energy Fuels 2016;30:10228–35. https://doi.org/10.1021/acs.energyfuels.6b01995.
[28] Ruiz-Morales Y, Alvarez-Ramírez F. Mesoscale Dissipative Particle Dynamics to Investigate Oil Asphaltenes and Sodium Naphthenates at the Oil−Water Interface. Energy Fuels 2021;35:9294–311. https://doi.org/10.1021/acs.energyfuels.1c00589.

[29] Goodarzi F, Zendehboudi S. Effects of Salt and Surfactant on Interfacial Characteristics of Water/Oil Systems: Molecular Dynamic Simulations and Dissipative Particle Dynamics. Ind Eng Chem Res 2019;58:8817–34. https://doi.org/10.1021/acs.iecr.9b00504.
[30] Alvarez F, Flores EA, Castro LV, Hernández JG, López A, Vázquez F. Dissipative Particle Dynamics (DPD) Study of Crude Oil−Water Emulsions in the Presence of a Functionalized Co-polymer. Energy Fuels 2011;25:562–7. https://doi.org/10.1021/ef1012038.
[31] Ruiz-Morales Y, Mullins OC. Coarse-Grained Molecular Simulations to Investigate Asphaltenes at the Oil–Water Interface. Energy Fuels 2015;29:1597–609. https://doi.org/10.1021/ef502766v.
[32] Zhang L, Shi C, Lu Q, Liu Q, Zeng H. Probing Molecular Interactions of Asphaltenes in Heptol Using a Surface Forces Apparatus: Implications on Stability of Water-in-Oil Emulsions. Langmuir 2016;32:4886–95. https://doi.org/10.1021/acs.langmuir.6b01000.
[33] Mozaffari S, Tchoukov P, Atias J, Czarnecki J, Nazemifard N. Effect of Asphaltene Aggregation on Rheological Properties of Diluted Athabasca Bitumen. Energy Fuels 2015;29:5595–9. https://doi.org/10.1021/acs.energyfuels.5b00918.
[34] Spoel DVD, Lindahl E, Hess B, Groenhof G, Mark AE, Berendsen HJC. GROMACS: Fast, flexible, and free. J Comput Chem 2005;26:1701–18. https://doi.org/10.1002/jcc.20291.
[35] Lindahl E, Hess B, van der Spoel D. Gromacs 3.0: A Package for Molecular Simulation and Trajectory Analysis. J Mol Model 2001;7:306–17. https://doi.org/10.1007/s008940100045.
[36] Berendsen HJC, van der Spoel D, van Drunen R. Gromacs: A Message-Passing Parallel Molecular Dynamics Implementation. Comput Phys Commun 1995;91:43–56. https://doi.org/10.1016/0010-4655(95)00042-E.
[37] Oostenbrink C, Villa A, Mark AE, Gunsteren WFV. A Biomolecular Force Field Based on the Free Enthalpy of Hydration and Solvation: The Gromos Force-Field Parameter Sets 53a5 and 53a6. J Comput Chem 2004;25:1656–76. https://doi.org/10.1002/jcc.20090.
[38] Sun X, Zeng H, Tang T. Effect of non-ionic surfactants on the adsorption of polycyclic aromatic compounds at water/oil interface: A molecular simulation study. J Colloid Interface Sci 2021;586:766–77. https://doi.org/10.1016/j.jcis.2020.10.146.
[39] Underwood TR, Greenwell HC. The Water-Alkane Interface at Various NaCl Salt Concentrations: A Molecular Dynamics Study of the Readily Available Force Fields. Sci Rep 2018;8:352. https://doi.org/10.1038/s41598-017-18633-y.
[40] Saito H, Nagao H, Nishikawa K, Kinugawa K. Molecular collective dynamics in solid para-hydrogen and ortho-deuterium: The Parrinello–Rahman-type path integral centroid molecular dynamics approach. J Chem Phys 2003;119:953–63. https://doi.org/10.1063/1.1578474.
[41] Hess B. P-LINCS: A Parallel Linear Constraint Solver for Molecular Simulation. J Chem Theory Comput 2008;4:116–22. https://doi.org/10.1021/ct700200b.
[42] Essmann U, Perera L, Berkowitz ML, Darden T, Lee H, Pedersen LG. A Smooth Particle Mesh Ewald Method. J Chem Phys 1995;103:8577–93. https://doi.org/10.1063/1.470117.
[43] van Buuren AR, Marrink SJ, Berendsen HJC. A molecular dynamics study of the decane/water interface. J Phys Chem 1993;97:9206–12. https://doi.org/10.1021/j100138a023.

[44] Hu C, Garcia NC, Xu R, Cao T, Yen A, Garner SA, et al. Interfacial Properties of Asphaltenes at the Heptol–Brine Interface. Energy Fuels 2016;30:80–7. https://doi.org/10.1021/acs.energyfuels.5b01855.
[45] Demond AH, Lindner AS. Estimation of interfacial tension between organic liquids and water. Environ Sci Technol 1993;27:2318–31. https://doi.org/10.1021/es00048a004.
[46] Pak CY, Li W, Steve Tse Y-L. Free Energy and Dynamics of Water Droplet Coalescence. J Phys Chem C 2018;122:22975–84. https://doi.org/10.1021/acs.jpcc.8b06507.
[47] Pak CY, Li W, Steve Tse Y-L. Free Energy and Dynamics of Organic-Coated Water Droplet Coalescence. J Phys Chem C 2020;124:8749–57. https://doi.org/10.1021/acs.jpcc.0c00175.
[48] Lemkul JA, Bevan DR. Assessing the Stability of Alzheimer's Amyloid Protofibrils Using Molecular Dynamics. J Phys Chem B 2010;114:1652–60. https://doi.org/10.1021/jp9110794.
[49] You W, Tang Z, Chang CA. Potential Mean Force from Umbrella Sampling Simulations: What Can We Learn and What Is Missed? J Chem Theory Comput 2019:11.
[50] Hub JS, de Groot BL, van der Spoel D. g_wham—A Free Weighted Histogram Analysis Implementation Including Robust Error and Autocorrelation Estimates. J Chem Theory Comput 2010;6:3713–20. https://doi.org/10.1021/ct100494z.
[51] Wang D, Yang D, Huang C, Huang Y, Yang D, Zhang H, et al. Stabilization mechanism and chemical demulsification of water-in-oil and oil-in-water emulsions in petroleum industry: A review. Fuel 2021;286:119390. https://doi.org/10.1016/j.fuel.2020.119390.
[52] Zhai X, Xu G, Chen Y, Liu T, Zhang J, Yuan J, et al. Effect of inorganic salts on the aggregation behavior of branched block polyether at air/water and n-heptane/water interfaces. Colloid Polym Sci 2013;291:2825–36. https://doi.org/10.1007/s00396-013-3013-y.
[53] Lashkarbolooki M, Ayatollahi S, Riazi M. The Impacts of Aqueous Ions on Interfacial Tension and Wettability of an Asphaltenic–Acidic Crude Oil Reservoir during Smart Water Injection. J Chem Eng Data 2014;59:3624–34. https://doi.org/10.1021/je500730e.
[54] Wang C, Wang X, Liu F, Jiang Z, Lin X. Surface concentration or surface excess, which one dominates the surface tension of multicomponent mixtures? Colloid Polym Sci 2018;296:89–93. https://doi.org/10.1007/s00396-017-4233-3.
[55] Kumar B. Effect of salinity on the interfacial tension of model and crude oil systems. University of Calgary, 2012.
[56] Hantal G, Sega M, Horvai G, Jedlovszky P. Role of the Counterions in the Surface Tension of Aqueous Surfactant Solutions. A Computer Simulation Study of Alkali Dodecyl Sulfate Systems. Colloids Interfaces 2020;4:15. https://doi.org/10.3390/colloids4020015.
[57] Kim S, Kim H, Choi J-H, Cho M. Ion aggregation in high salt solutions: Ion network versus ion cluster. J Chem Phys 2014;141:124510. https://doi.org/10.1063/1.4896227.
[58] Choi J-H, Cho M. Ion aggregation in high salt solutions. IV. Graph-theoretical analyses of ion aggregate structure and water hydrogen bonding network. J Chem Phys 2015;143:104110. https://doi.org/10.1063/1.4930608.
[59] Choi J-H, Cho M. Ion aggregation in high salt solutions. II. Spectral graph analysis of water hydrogen-bonding network and ion aggregate structures. J Chem Phys 2014;141:154502. https://doi.org/10.1063/1.4897638.

[60] Ballal D, Srivastava R. Modeling the interfacial properties of Poly(Ethylene oxide-Co-Propylene oxide) polymers at water-toluene interface. Fluid Phase Equilibria 2016;427:209–18. https://doi.org/10.1016/j.fluid.2016.07.013.
[61] Horváth-Szabó G, Masliyah JH, Elliott JAW, Yarranton HW, Czarnecki J. Adsorption isotherms of associating asphaltenes at oil/water interfaces based on the dependence of interfacial tension on solvent activity. J Colloid Interface Sci 2005;283:5–17. https://doi.org/10.1016/j.jcis.2004.08.174.
[62] Remesal ER, Suárez JA, Márquez AM, Sanz JFdez, Rincón C, Guitián J. Molecular dynamics simulations of the role of salinity and temperature on the hydrocarbon/water interfacial tension. Theor Chem Acc 2017;136:66. https://doi.org/10.1007/s00214-017-2096-9.
[63] Tadros T. Gibbs Adsorption Isotherm. In: Tadros T, editor. Encycl. Colloid Interface Sci., Berlin, Heidelberg: Springer Berlin Heidelberg; 2013, p. 626–626. https://doi.org/10.1007/978-3-642-20665-8_97.
[64] Jian C, Poopari MR, Liu Q, Zerpa N, Zeng H, Tang T. Reduction of Water/Oil Interfacial Tension by Model Asphaltenes: The Governing Role of Surface Concentration. J Phys Chem B 2016;120:5646–54. https://doi.org/10.1021/acs.jpcb.6b03691.
[65] Li W, Nan Y, Wen X, Wang W, Jin Z. Effects of Salinity and N-, S-, and O-Bearing Polar Components on Light Oil–Brine Interfacial Properties from Molecular Perspectives. J Phys Chem C 2019;123:23520–8. https://doi.org/10.1021/acs.jpcc.9b06600.
[66] Soleymanzadeh A, Rahmati A, Yousefi M, Roshani B. Theoretical and experimental investigation of effect of salinity and asphaltene on IFT of brine and live oil samples. J Pet Explor Prod Technol 2020. https://doi.org/10.1007/s13202-020-01020-1.
[67] Rodríguez-Hakim M, Anand S, Tajuelo J, Yao Z, Kannan A, Fuller GG. Asphaltene-induced spontaneous emulsification: Effects of interfacial co-adsorption and viscoelasticity. J Rheol 2020;64:799–816. https://doi.org/10.1122/1.5145307.